

## Full-atomistic simulations of poly( $\epsilon$ -caprolactone) diol models with CVFF and CGenFF

Yin Chang and Shu-Wei Chang\*

Department of Civil Engineering, National Taiwan University, Civil Engineering Research Building  
No.188, Sec. 3, Sinhai Rd., Da-an District, Taipei 10668, Taiwan

(Received September 9, 2016, Revised October 6, 2016, Accepted October 10, 2016)

**Abstract.** Poly( $\epsilon$ -caprolactone) (PCL) diol, with good biodegradation and biocompatibility, is one of the widely used soft segments (SSs) in composing bio-polyester-urethanes (Bio-PU), which show great potential in both biomedical and tissue engineering applications. Properties of Bio-PU are tunable by combining SS monomers with different molecular weights, structures, modifications, and ratio of components. Although numbers of research have reported many Bio-PU properties, few studies have been done at the molecular scale. In this study, we use molecular dynamic (MD) simulation to construct atomistic models for two commonly used PCL diol SSs with different molecular weights 1247.58 Da and 1932.42 Da. We compare the simulation results by using two widely used classical force fields for organic molecules: Consistent Valence Force Field (CVFF) and CHARMM General Force Field (CGenFF), and discuss the validity and accuracy. Melt density, volume, polymer conformations, transition temperature, and mechanical properties of PCL diols are calculated and compared with experiments. Our results show that both force fields provide accurate predictions on the properties of PCL diol system at the molecular scale and could help the design of future Bio-PU.

**Keywords:** Molecular dynamic (MD); Poly( $\epsilon$ -caprolactone) (PCL) diol; Consistent Valence Force Field (CVFF); CHARMM General Force Field (CGenFF)

### 1. Introduction

Experiments and simulation studies on the interactions between amino acids, solvents, and synthetic molecules are important in developing cell culture scaffolds, drug delivery matrix, or implant stents. Biodegradable Polyurethanes (Bio-PU) have been used as building blocks for fabricating various tissue scaffolds in biomedical fields (Lim *et al.* 2013, Martina and Hutmacher 2007, Ou *et al.* 2014, Tatai *et al.* 2007). Being implanted or injected into human body, the thermal stability and mechanical properties of Bio-PU under human body temperature have been studied (Fakirov 2006, Marcos-Fernández *et al.* 2006, Tiwari and Raj 2015). Bio-PU are created by using dialcohol materials as soft segments and combine with hard segments diisocyanate. PCL diol is one of the commonly used soft segments in Bio-PU. PCL diol is relatively cheap, and is with

---

\*Corresponding author, Professor, E-mail: changsw@ntu.edu.tw

good thermal stability and biocompatibility, which have been approved by Food and Drug Administration for clinical use (Labet and Thielemans 2009, Sinha *et al.* 2004).

Moreover, the mechanical properties can be tuned by combining PCL diols with different molecular weights (Tatai *et al.* 2007), or different combination ratio of hard segments (Karchin *et al.* 2011, Li and Tan 2014, Marcos-Fernández *et al.* 2006). Therefore, in recent years, diverse PCL diol Bio-PUes have been synthesized to provide required properties in biomedical applications (Chen and Hsu 2014, Gref *et al.* 1994, Hsu *et al.* 2014, Niu *et al.* 2014, Younes *et al.* 2004).

Numbers of experimental and theoretical approaches have been conducted to evaluate the microstructures (Iwata and Doi 2002, Iwata *et al.* 2004, Kweon *et al.* 2003, Li *et al.* 2011, Ou *et al.* 2014), crystallinity (Bittiger *et al.* 1970, Chatani *et al.* 1970, Fuller *et al.* 1942), thermal properties, and mechanical responses (Chatani *et al.* 1970) of PCL-based materials. Interaction between PCL-based materials and biomolecules such as enzymatic behavior (Fuller *et al.* 1942), degradability (Chatani *et al.* 1970, Iwata *et al.* 2004), and biocompatibility (Bittiger *et al.* 1970) have been investigated. However, properties at ultrafine- or nano-scale are hard to be quantified. Therefore, the interactions between biomolecules and the PCL-based materials at nano-scale are still not well understood (Uemura *et al.* 2010).

Computational approaches such as density functional theory (DFT) (Ballone *et al.* 1999, Montanari *et al.* 1999), Monte Carlo (Pandey *et al.* 2009), and molecular dynamics (MD) (Bhowmik *et al.* 2007, Feng *et al.* 2011, Li *et al.* 2011, Regis *et al.* 2014) have been used to explore conformational changes and mechanical responses of polymeric scaffolds. Force fields describe molecule conformation such as atom types, bond types, topology, and the energy of the molecular model. Therefore, the selection of force field is determinant to the accuracy of simulation results of specific system. For example, Consistent Valence Force Field (CVFF) (Maple *et al.* 1988), CHARMM, and CHARMM General Force Field (CGenFF) (Vanommeslaeghe *et al.* 2010) have been used for a variety of functional groups such as amino acids, hydrocarbons, and water (Molecular Simulations 1998, Studio. 2002-2016). On the other hand, several groups have explored the validity of PCL-based models with CVFF. For example, Rahul Bhowmik has reported good applicability of CVFF parameters in evaluating interactions between PCL polymer and hydroxyapatite (HA) (Bhowmik *et al.* 2007). Quanshun *et al.* have derived consistent simulation results of enzyme-PCL interaction energy with experimental data (Li *et al.* 2011). Both force fields have been applied to compute biological properties such as hydrogen bonds (Lifson *et al.* 1979), pKa shift, free energies between solvent and amino acids (Dixit *et al.* 1997), or interactions between metal and amino acids (Feng *et al.* 2011). For example, Surjit *et al.* have compared the experimental solvation energy of each amino acid with computational results based on AMBER, CHARMM, CVFF, GROMOS, OPLS, PARSE, and ab initio-derived charges. They have concluded that among those force fields, CHARMM force field results in least overall deviation of calculated results and experiment data (Dixit *et al.* 1997).

CGenFF is an extensive force field of CHARMM and is applicable to both biomolecules and drug-like functional groups. The compatibility of modeling drug-like molecules in CGenFF and biomolecules in CHARMM force fields benefit for modeling interactions between chemical molecules and biomolecules. Although both CVFF and CGenFF have been used for simulating polymer systems, the accuracy and applicability of CVFF and CGenFF for PCL diol polymers have not been carefully studied. Therefore, in this study, we use MD simulation to study the properties of PCL diol models with different molecular weights. Structural characteristics including polymer melt density, volume, conformations, transition temperature, and thermal characteristics are calculated and discussed. We compare the calculated properties of PCL diol in

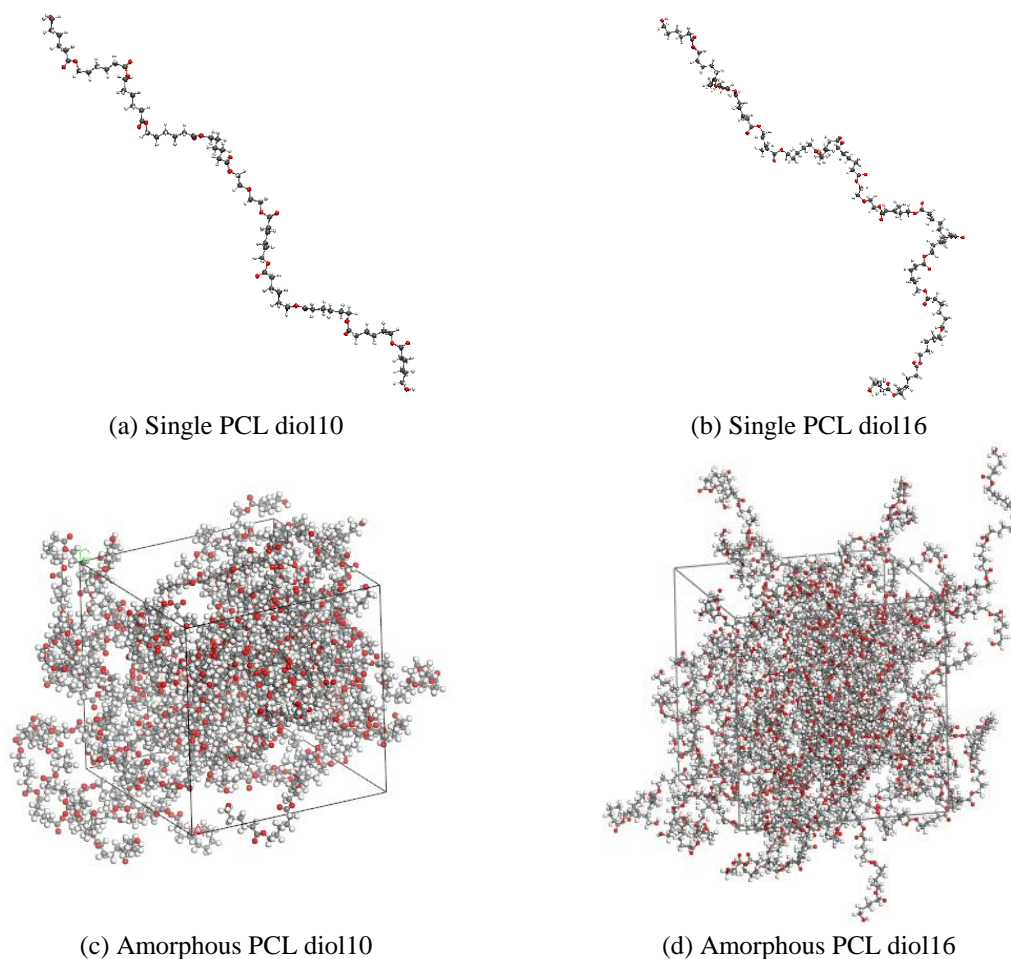


Fig 1. (a) Single PCL diol10 model:  $C_{64}H_{110}O_{23}$  with total 197 atoms (b) Single PCL diol16 model:  $C_{100}H_{170}O_{35}$ , with total 305 atoms (c) Amorphous PCL diol10 model with initial density=  $1.07 \text{ g/cm}^3$ , box size= $37.39\text{\AA} \times 37.39\text{\AA} \times 37.39\text{\AA}$ , initial volume=  $52.275 \text{ nm}^3$  (d) Amorphous PCL diol16 model with initial density=  $1.07 \text{ g/cm}^3$ , Box:  $43.26\text{\AA} \times 43.26\text{\AA} \times 43.26\text{\AA}$ , initial volume=  $80.958 \text{ nm}^3$

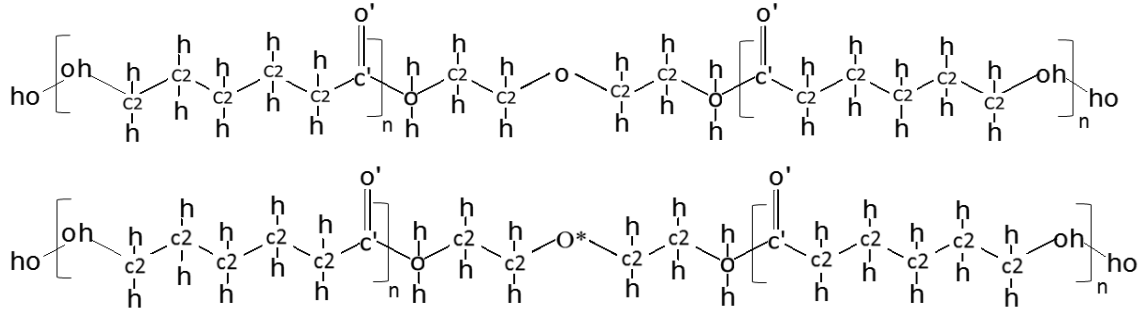
both dilute and melt polymer systems based on CVFF and CGenFF. By comparing with experimental data, we examine the accuracy and applicability of both force fields.

## 2. Simulation details

### 2.1 Model construction

Fig. 1 shows the conformation of PCL diol models constructed in this study. Fig. 1 (a) (b) show single PCL diol polymer chain,  $(C_6H_{10}O_2)_{2n}$ , with two molecular weights: PCLdiol10, ( $n=5$ ,  $M_w \sim 1247.58 \text{ Da}$ , i.e. total 10 chemical repeat units) and PCLdiol16 ( $n=8$ ,  $M_w \sim 1932.42 \text{ Da}$ , i.e. total 16 chemical repeat units). Initial amorphous models for polymer melt systems, constructed by

Table 1 Illustrations of atom types and bond coefficient used to parameterize PCL diol system in CVFF (top) and CHARMM force field (bottom). Corresponding chemical conformation and atom positions are illustrated as the chemical formula. For both force fields, bond energy is calculated by  $E(\text{bond}) = K_b (r - r_{\text{eq}})^2$



Bond	O*-c2	o-c2	o-c'	oh-c2	oh-ho	c'-c2	c'-o'	c2-c2	c2-h
CVFF									
$r_{\text{eq}}$ (Å)		1.425	1.37	1.42	0.96	1.52	1.23	1.526	1.105
$K_b$ (Kcal/mol)		273.20	400.00	384.00	540.63	283.09	615.32	322.72	340.6175
CHARMM36									
$r_{\text{eq}}$ (Å)	1.415	1.44	1.334	1.42	0.96	1.522	1.22	1.53	1.111
$K_b$ (Kcal/mol)	360	320	150	428	545	200	750	222.5	309

the Amorphous cell module (Accelrys Inc, Material Studio 8.0, 2002-2016), are comprised by 27 entangled PCL diol chains with an initial density of  $1.07 \text{ g/cm}^3$  at room temperature ( $T = 300 \text{ K}$ ). Amorphous models are constructed as shown in Figure 1 (c) (d), and are both with 27 chains in cubic simulation boxes. The side length of the simulation box of PCLdiol10 is  $37 \text{ \AA}$  (containing 5319 atoms). The side length of the simulation box of PCLdiol16 is  $43 \text{ \AA}$  (containing 8235 atoms). In this study, the dilute system means there is no interaction between each ideal polymer chain. Dense melt system means there are entanglement and interactions between each polymer chain.

## 2.2 Force field setting

For CGenFF parameterization, the charges and potentials for every atom type is acquired through uploading the monomer of PCL diol to the website of Paramchem (Vanommeslaeghe *et al.* 2011, Vanommeslaeghe *et al.* 2012). Topology and parameters are generated by CGenFF version 3.0.1 (Vanommeslaeghe *et al.* 2010, Yu *et al.* 2012). For CVFF parameterization, parameters including bonded, non-bonded, and partial charges are taken from CVFF version 2.4 (Dauberosguthorpe *et al.* 1988). CVFF treats PCL diol model with 7 atom types, whereas CHARMM distinguishes 8 atom types. The atom types found in both force fields are labeled in Table 1.

## 2.3 MD Procedures

Full-atomistic models: PCL diol chains with two molecular weights in dilute and melt systems are simulated using LAMMPS program (Plimpton and Hendrickson 1995). Melt system is set with

periodic boundary condition, and the long-range electrostatic interactions are computed by the particle-particle particle-mesh (PPPM) method. Atomic neighbor list and cut-off criteria are with different settings for fitting the parameters and functional forms in the two force fields respectively. CVFF parameterized models are set with Lennard-Jones interactions cut-off radius of 10 Å and columbic interactions cut-off radius of 8 Å, while CGenFF parameterized models are with inner cut-off 8 Å and outer cut-off 10 Å. Processes of energy minimization, canonical ensemble (NVT), and isothermal-isobaric (NPT) ensemble are employed to these models. Temperature is controlled by Nose-Hoover thermostat. Geometry of each model is first optimized through energy minimization with steepest descent algorithm. In simulating dilute system, the model is then simulated with NVT ensemble at different temperature from 100k to 800k for 1ns.

For simulating the polymer melt system, after NVT ensemble process, the equilibrium configurations are then performed NPT ensemble with isobaric pressure setting at 1 atm and constant temperature holding at 100 K, 200K, 300K, 310K, 320K, 325K, 350K, 400K, 500K, 600K, 700K, 800K separately for 1 ns. Enthalpy and Van der Waals energy analysis of polymer melt system at different temperatures are then calculated and compared with both force fields.

## 2.4 Analyzing methods

### 2.4.1 Radius of gyration and end to end distance of single chain

Radius of gyration and end to end distance are two critical indicators of polymer geometry and intrinsic properties such as flexibility. The radius of gyration of a polymer is calculated as the root mean square distance of each atom with their mass center, which is calculated by Eq. (1).

$$r_g^2 = \left( \sum_{i=1}^n w(i)(r(i) - \bar{r})^2 \right) / \left( \sum_{i=1}^n w(i) \right) \quad (1)$$

where  $r(i)$  is the position of the  $i^{\text{th}}$  atom and  $\bar{r}$  is the position of mass center.

End to end distance is estimated by the distance between the first and the last atoms of each chain, i.e.  $\|oh_n - oh_1\|$ , where n refers to the nth repeated segment.

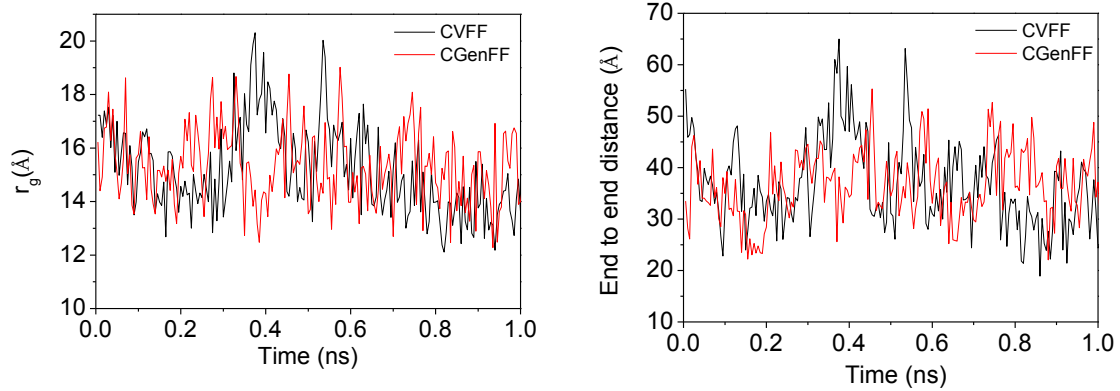
### 2.4.2 Transition temperature of polymer melt

Transition temperature (softening point,  $T_{tr}$ ) is a unique property of polymers. When polymers are with surrounding temperature below  $T_{tr}$ , they behave like glass that is hard and brittle. When above  $T_{tr}$ , polymers perform like rubber that is soft and viscous. Although polymers possess two completely different states below or above  $T_{tr}$ , transition is a second order transition process so that many first order properties such as volume and enthalpy would change gradually with increasing temperature. Therefore,  $T_{tr}$  can be derived from fitting intercept of the two linear trend lines at low and high temperature respectively.

### 2.4.3 Persistence length and stiffness of single chain

To estimate the contour length ( $L_c$ ) and the end to end distance of the molecules, we compute the bond length ( $l_i$ ) of the neighbor atoms in the main chain, i.e. oh, c2, c', o, O\*, then the contour length is the summation of these distances of total segments (n), i.e.  $L_c = \sum_i^n l_i$  ( $L_c \sim 115\text{\AA}$  for single PCL diol chain)

Persistence length ( $L_p$ ) is a characterization of single polymer chain, and could be used to



(a) Radius of gyration of single PCLdiol10 calculated by CVFF (black) and CGenFF (red)

(b) End to end distance of single PCLdiol10 calculated by CVFF (black) and CGenFF (red)

Fig. 2 CVFF and CGenFF calculated PCL diol10 structural characteristics at 300 K in dilute system for the last 0.5ns at 300 K. (a) Radius of gyration (b) end to end distance of single polymer chain.

estimate the mechanical properties of a polymer chain such as stiffness. We use the following equation to derive  $L_p$  by considering rotating angles, end to end distance ( $\mathbf{r}$ ), and contour length

$$\langle \mathbf{r}^2 \rangle = 2\langle L_c \rangle L_p + 2L_p^2 (1 - e^{-\langle L_c \rangle / L_p}) \quad (2)$$

The bending stiffness  $B$  of a polymer can be calculate from its persistence length by the relation  $L_p = B/k_B T$ , where  $k_B$  is Boltzmann's constant and  $T$  is the absolute temperature. The Young's modulus  $E$  of a polymer can be calculated by  $E = L_p k_B T / I$ , where  $B = EI$ , in which  $I$  is the second moment of area of the polymer. (The diameter of polymer chain is assumed to be 4 Å for all models).

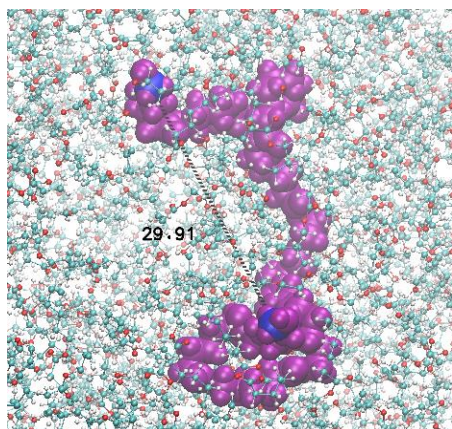
### 3. Results and discussions

#### 3.1 Structure characteristics of PCLdiol10 chain in dilute system

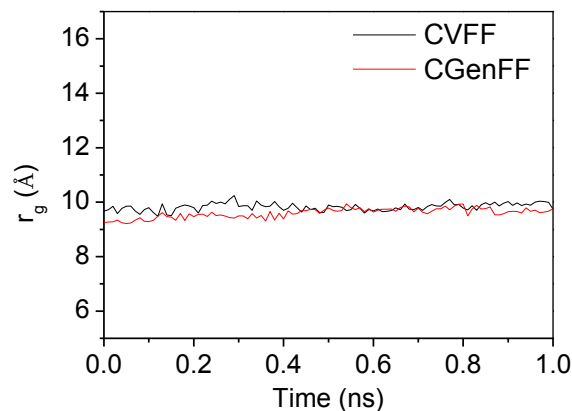
Fig. 2(a), (b) show the radius of gyration ( $r_g$ ) and the end to end distance of single chain in dilute PCLdiol10 system at 300 K. Both CVFF and CGenFF simulation results show similar geometry features of PCLdiol10. For example,  $r_g$  of PCLdiol10 is  $\sim 14.87 \pm 1.67$  Å for CVFF, and is  $\sim 15.23 \pm 1.36$  Å for CGenFF. End to end distance of PCLdiol10 is  $\sim 35.93 \pm 8.15$  Å for CVFF, and is  $\sim 37.10 \pm 5.72$  Å for CGenFF. From the results, we find out that both force fields show that  $r_g$  is smaller than the root mean square of end to end distance by a factor of  $\sim \sqrt{6}$ , which indicates that, in dilute system, the single PCL diol chain could be described with an equivalent freely joined chain model (Kuhn and Kuhn 1943).

#### 3.2 Structure characteristics of PCLdiol10 chain in dense polymer melt

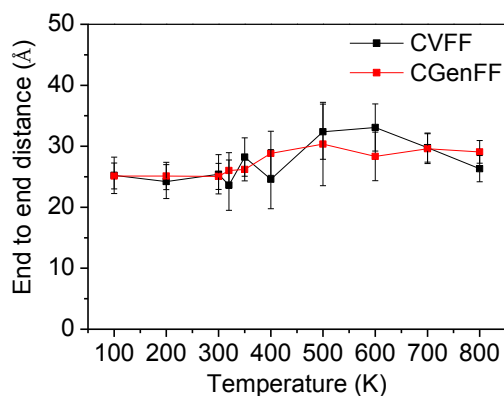
Fig. 3(a) illustrates the end to end measurement of single polymer chain in polymer melt system. Fig. 3(b) shows  $r_g$  of single PCLdiol10 chain is  $\sim 9.82 \pm 0.14$  Å with CVFF, and is  $9.60 \pm$



(a) End to end distance measurement of single PCL diol polymer



(b) Radius of gyration of single PCLdiol10 chain in melt system calculated by CVFF (black) and CGenFF (red)



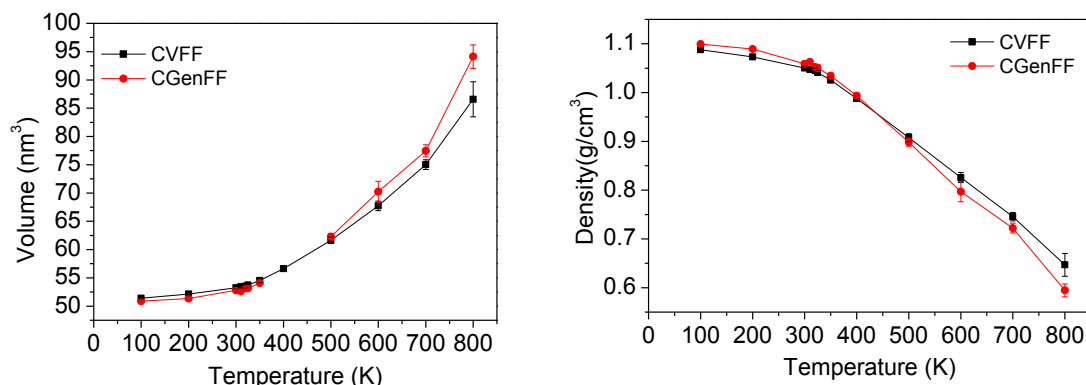
(c) End to end distance of single PCLdiol10 chain in melt system calculated by CVFF (black) and CGenFF (red)

Fig 3. Single PCLdiol10 polymer chain structural characteristics in melt system with CVFF (black line) and CGenFF (red line) (a) Illustration of end to end distance measurement (unit: Å). (b) radius of gyration (c) end to end distance of PCLdiol10 single chain at temperature from 100 to 800K.

0.18 Å with CGenFF.

It could be observed from Fig. 3(b), (c), both mean value and variation of measured  $r_g$  of single PCLdiol10 polymer chain in melt system is much smaller than those in dilute system (Figure 2 (a)). This reflects the entanglements of polymer chains in high concentration polymer melt. The results also imply that the mobility of single polymer in a polymer melt is restricted by the presence of neighboring chains.

Fig. 3(c) shows the relations between end to end distance and temperature from 100 to 800 K. It could be observed that for both CVFF and CGenFF, the end to end distance of single chain in polymer melt appears to be insensitive to temperature below 300 K and above 500 K, but is with increasing values from 300 K to 500 K. Comparatively, as shown in Fig. 4, we can see that volume of polymer melt system is temperature dependent. Moreover, larger thermal expansion coefficient of PCL diol can be observed when temperature rises above ~310 K.



(a) Volume of PCL diol10 polymer melt calculated by CVFF (black) and CGenFF (red) (b) Density of PCL diol10 polymer melt calculated by CVFF (black) and CGenFF (red)

Fig. 4(a) Volume and (b) density of PCL diol10 polymer melt at different temperatures calculated by CVFF and CGenFF. The two force fields simulation results are with almost the same values at around 300 K, but CGenFF derived slightly larger value of volume at high temperature.

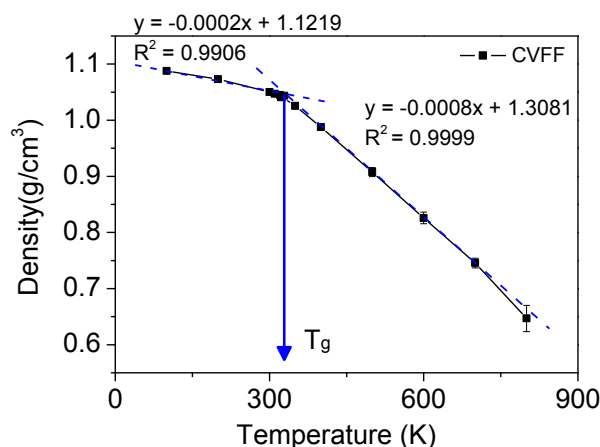


Fig. 5  $T_{tr}$  fitted by intersecting two linear trend lines at low and high temperature

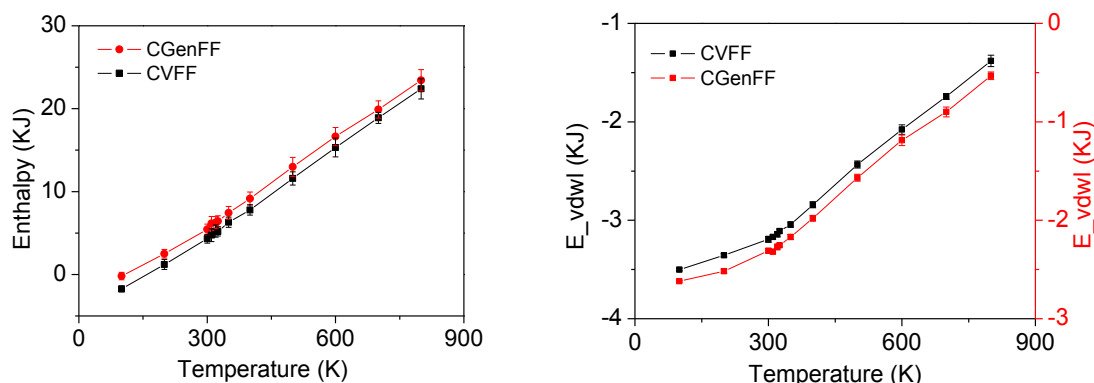
### 3.3 Transition temperature of PCLdiol10 and PCLdiol16

The fitting results of transition temperature are shown in Fig. 5. The two fitted linear trend lines show  $R^2 \sim 0.99$  referring density of PCL diols change linearly with temperature. Calculated  $T_{tr}$  and density are listed in Table 2 and compared with experimental data from marketing PCL diol products provided by Sigma-Aldrich Corporation. The density of PCLdiol10 and PCLdiol16 calculated by CVFF and CGenFF also fit well with the experimental value (1.071 g/cm<sup>3</sup>). For  $T_{tr}$  estimations, both CVFF and CGenFF show an abrupt bend of the volume of polymer melt at  $T_{tr}$  value ( $\sim 318$  K for PCLdiol10 and  $\sim 320$  K for PCLdiol16). Marginal differences of  $T_{tr}$  and density of PCL diols between simulation and experiment results reveal that both CVFF and CGenFF provide accurate prediction in calculating PCL diol structural characteristics and thermal responses. To look at the simulation result in detail, CVFF and CGenFF fit very well around 300 K and at lower temperature, but are with larger deviation at high temperature.



Table 2 Density and  $T_{tr}$  of PCL diol10 and PCL diol16 calculated by CVFF and CGenFF. Both force fields derive close values of density and  $T_{tr}$  with relatively small deviation points out their good applicability in parameterizing and calculating polymer system. (\*Experimental data are from marketing PCL diol products provided by Sigma-Aldrich Corporation.)

	$\rho$ (g/cm <sup>3</sup> )	$T_g$ (K)
Experiment		
PCLdiol10*	1.071 (298 K)	318
PCLdiol16*	1.071 (298 K)	323
CVFF		
PCLdiol10	1.05 $\pm$ 0.004 (300 K)	320.22 $\pm$ 4.806
PCLdiol16	1.05 $\pm$ 0.003 (300 K)	323.75 $\pm$ 6.885
CHARMM		
PCLdiol10	1.06 $\pm$ 0.003 (300 K)	319.39 $\pm$ 7.536
PCLdiol16	1.07 $\pm$ 0.003 (300 K)	321.19 $\pm$ 6.170



(a) Enthalpy of PCLdiol10 polymer melt calculated by CVFF (black) and CGenFF (red)

(b) Van der Waals energy of PCLdiol10 polymer melt calculated by CVFF (black) and CGenFF (red)

Fig. 6 Bonded and nonbonded energy at different temperature calculated by CVFF and CGenFF. (a) Bonded energy (enthalpy) at different temperature. (b) Nonbonded energy values ( $E_{vdwl}$ ) calculated by CGenFF are around 1250 J higher than those calculated by CVFF at all ranges of temperature.

### 3.4 Thermodynamic responses of PCL diol system

Transition of amorphous phase polymer is a second order transition process that means many first order properties such as volume (Fig. 4) and energy (Fig. 6) change continually with increasing temperature. Moreover, despite CVFF and CGenFF report different atom types and bond coefficients (Table 1), similar bond energy (Fig. 6(a)) and non-bond energy (Fig. 6(b)) are derived from the two force fields. This means energy-temperature relation calculated by the two force fields are almost the same. Our simulation process well describes the second-order transition characteristics of polymer melt, which confirms the validity of MD simulation with both CVFF and CGenFF in calculating condensed polymeric system.

Table 3 Simulated mechanical properties of PCLdiol 10 and PCLdiol16 in dilute and concentrated condition calculated in this study, and experimental properties of electrospun PCL fibers provided by other research groups.

Ref.	Fiber type	Molecular weight (KDa)	Diameter (nm)	Lc (nm)	Young's Modulus (Mpa)
This study	Dilute PCLdiol10 (300k), CVFF	1.25	0.40	11.5	1833.38± 769.97
	Dilute PCLdiol10 (300k), CGenFF	1.25	0.40	11.5	1907.78± 559.28
	Dilute PCLdiol16 (300k), CVFF	1.93	0.40	17.6	170.46± 75.25
	Dilute PCLdiol16 (300k), CGenFF	1.93	0.40	17.6	104.16± 133.36
	Melt PCLdiol10 (300k), CVFF	1.25	0.40	11.5	523.25± 61.23
	Melt PCLdiol10 (300k), CGenFF	1.25	0.40	11.5	911.53± 140.71
	Melt PCLdiol16 (300k), CVFF	1.93	0.40	17.6	1450.31± 72.50
	Melt PCLdiol16 (300k), CGenFF	1.93	0.40	17.6	1266.18± 133.09
Bhowmik, 2008	SMD, Single polyacrylic acid (PAAc), CHARMM	1.01	-	-	~37710
Baker, 2016	Electrospun PCL fibers	120–300	440–1040	-	62.3 ± 25.6
	Electrospun PCL fibers	60	200-300	-	2000-3250
Tan, 2005	Electrospun PCL fibers	80	1100–1700	-	120 ± 30
Wong, 2008	Electrospun PCL fibers	80	350–2500	-	275
Chew, 2006	Electrospun PCL fibers	60	230–5000	-	1000-3000
	PCL film	86-89	Thickness: 5mm	-	330-570
Crosier, 2012	Electrospun PCL fibers	80	250–700	-	3700 ± 700

In addition, according to the results of temperature dependency of single polymer chain end to end distance (Fig. 3(c)) and polymer melt volume expansion (Fig. 4), we find out that higher temperature causes larger inter-chain distance but does not change the constraints of single chain movement which renders the whole polymer melt system in a less compact conformation.

### 3.5 Mechanical property of single PCLdiol10 and PCLdiol16

We derive stiffness of single PCL diol chain from simulating results of persistence length at 300 K. The average values and deviations of each model with CVFF and CGenFF in different concentrations are listed in Table 3. In addition, we review and organize experimental data of Young's modulus of PCL-based materials provided by other research groups.

As listed in Table 3, our simulation results with both CVFF and CGenFF show that in dilute system, PCLdiol10 possess an order of magnitude higher stiffness than PCLdiol16. However, in melt system, both force fields calculate higher stiffness of PCLdiol16 than PCLdiol10. The high

stiffness in melt system might be caused by both the nature of themselves and the entanglements with neighbors. Another interesting phenomenon is that both force fields show in dilute condition, PCLdiol10 polymer chains possess higher stiffness, but PCLdiol16 chains possess lower stiffness. This implies the entanglements of PCLdiol16 might be more significant.

Our computational results show all our PCLdiol models possess stiffness an order of magnitude smaller than the one calculated through SMD ( $\sim 37710$  MPa) (Bhowmik *et al.* 2008). However, our results are comparable with other experimental data that stiffness of PCL-based materials range from 102 to 103 MPa. Baker's group concluded that Young's modulus for single electrospun fibers would increase as the fiber diameter decreases to nanoscale. They also revealed that the properties of single fiber would approach that of the bulk as fiber diameter increases. For example, Young's modulus of PCL film ( $\sim 330$ - $570$  MPa) reported by Chew's group was about 5 times higher than the PCL nanofiber ( $\sim 62.3 \pm 25.6$  MPa) reported by Baker (2016).

#### 4. Conclusions

We consider two classical force fields: CVFF and CGenFF for PCL diol polymers in dilute and in melt (condensed phase) systems. We calculate the static structure, thermal properties, and mechanical properties of PCLdiol10 and PCLdiol16. We find that CVFF and CGenFF show no structural differences in describing the single chain geometry ( $r_g$  and end to end distance) in both dilute and melt system. Both force fields also show similar energy characteristics, thermodynamic responses, and mechanical properties of PCL diols.

The accuracy and applicability of CVFF and CGenFF are discussed based on comparing  $T_{tr}$  and mechanical properties of both PCLdiol10 and PCLdiol16 with experimental data. The calculated mechanical properties of single PCL diol chains show similar results for CVFF and CGenFF. The calculated stiffness of PCLdiol10 and PCLdiol16 are comparable to experimental data ranging from 102 to 103 MPa. We also confirm that PCL diol with shorter monomer units (PCLdiol10) has higher stiffness in dilute system.

Our results show that CVFF and CGenFF are both applicable to PCL diol in computing transition temperature and thermodynamic responses. The applicability and accuracy of CGenFF on synthetic polymers will open up more chances for simulating various synthetic chemical molecules and for predicting the interactions between chemical molecules and biomolecules.

#### Acknowledgments

This research is supported by Ministry of Science and Technology (MOST 104-2218-E-002-035), Taiwan, R.O.C. and an international cutting-edge research project supported by National Taiwan University (NTU-ICRP-105R7564) under the Center of Tissue Engineering and 3D Printing.

#### References

Baker, S.R., Banerjee, S., Bonin, K. and Guthold, M. (2016), "Determining the mechanical properties of electrospun Poly-E-Caprolactone (Pcl) nanofibers using Afm and a novel fiber anchoring technique",

- Mater. Sci. Eng.*, **C59**, 203-212.
- Ballone, P., Montanari, B., Jones, R.O. and Hahn, O. (1999), "Polycarbonate simulations with a density functional based force field", *J. Phys. Chem.*, **A103**(27), 5387-5398.
- Bhowmik, R., Katti, K.S. and Katti, D.R. (2008), "Influence of mineral on the load deformation behavior of polymer in Hydroxyapatite-Polyacrylic acid nanocomposite biomaterials: A steered molecular dynamics study", *J. Nanosci. Nanotech.*, **8**(4), 2075-2084.
- Bhowmik, R., Katti, K.S., Verma, D. and Katti, D.R. (2007), "Probing molecular interactions in bone biomaterials: Through molecular dynamics and fourier transform infrared spectroscopy", *Mater. Sci. Eng.*, **C27**(3), 352-371.
- Bittiger, H., Marchessault, R.H. and Niegisch, W.D. (1970), "Crystal structure of Poly-[Epsilon]-caprolactone", *Acta Crystallographica Section B*, **26**(12), 1923-1927.
- Chatani, Y., Okita, Y., Tadokoro, H. and Yamashita, Y. (1970), "Structural studies of polyesters. Iii. Crystal structure of Poly-[Epsi]-Caprolactone", *Polym. J.*, **1**(5), 555-562.
- Chen, Y.P. and Hsu, S.H. (2014), "Preparation and characterization of novel water-based biodegradable polyurethane nanoparticles encapsulating superparamagnetic iron oxide and hydrophobic drugs", *J. Mater. Chem. B*, **2**(21), 3391-3401.
- Dauberosguthorpe, P., Roberts, V.A., Osguthorpe, D.J., Wolff, J., Genest, M. and Hagler, A.T. (1988), "Structure and energetics of ligand-binding to proteins - Escherichia-coli dihydrofolate reductase trimethoprim, a drug-receptor system", *Proteins-Struct. Funct. Genetics*, **4**(1), 31-47.
- Dixit, S.B., Bhasin, R., Rajasekaran, E. and Jayaram, B. (1997), "Solvation thermodynamics of amino acids assessment of the electrostatic contribution and force-field dependence", *J. Chem. Soc. Faraday Transactions*, **93**(6), 1105-1113.
- Fakirov, S. (2006), *Handbook of Condensation Thermoplastic Elastomers*, Wiley.
- Feng, J., Pandey, R.B., Berry, R.J., Farmer, B.L., Naik, R.R. and Heinz, H. (2011), "Adsorption mechanism of single amino acid and surfactant molecules to au {111} Surfaces in aqueous solution: Design rules for metal-binding molecules", *Soft Matter*, **7**(5), 2113-2120.
- Fuller, C.S., Frosch, C.J. and Pape, N.R. (1942), "Chain structure of linear polyesters - Trimethylene Glycol series", *J. Am. Chem. Soc.*, **64**(1), 154-160.
- Gref, R., Minamitake, Y., Peracchia, M.T., Trubetskoy, V., Torchilin, V. and Langer, R. (1994), "Biodegradable long-circulating polymeric nanospheres", *Sci.*, **263**(5153), 1600-1603.
- Hsu, S.H., Hung, K.C., Lin, Y.Y., Su, C.H., Yeh, H.Y., Jeng, U.S., Lu, C.Y., Dai, S.H.A., Fu, W.E. and Lin, J.C. (2014), "Water-based synthesis and processing of novel biodegradable elastomers for medical applications", *J. Mater. Chem. B*, **2**(31), 5083-5092.
- Iwata, T. and Doi, Y. (2002), "Morphology and enzymatic degradation of Poly( $\epsilon$ -Caprolactone) single crystals: Does a polymer single crystal consist of micro-crystals?" *Polym. Int.*, **51**(10), 852-858.
- Iwata, T., Kobayashi, S., Tabata, K., Yonezawa, N. and Doi, Y. (2004), "Crystal structure, thermal behavior and enzymatic degradation of Poly(Tetramethylene Adipate) solution-grown chain-folded lamellar crystals", *Macromole. Biosci.*, **4**(3), 296-307.
- Karchin, A., Simonovsky, F.I., Ratner, B.D. and Sanders, J.E. (2011), "Melt electrospinning of biodegradable polyurethane scaffolds", *Acta Biomater.*, **7**(9), 3277-3284.
- Kuhn, W. and Kuhn, H. (1943), "The question after the recalculation of thread molecules in flowing solutions", *Helv Chim Acta*, **26**, 1394-1465.
- Kweon, H., Yoo, M.K., Park, I.K., Kim, T.H., Lee, H.C., Lee, H.S., Oh, J.S., Akaike, T. and Cho, C.S. (2003), "A novel degradable polycaprolactone networks for tissue engineering", *Biomater.*, **24**(5), 801-808.
- Labet, M. and Thielemans, W. (2009), "Synthesis of polycaprolactone: A review", *Chem. Soc. Rev.*, **38**(12), 3484-3504.
- Li, Q., Li, G., Yu, S., Zhang, Z., Ma, F. and Feng, Y. (2011), "Ring-opening polymerization of  $\epsilon$ -caprolactone catalyzed by a novel thermophilic lipase from *Fervidobacterium nodosum*", *Process Biochem.*, **46**(1), 253-257.
- Li, Z. and Tan, B.H. (2014), "Towards the development of polycaprolactone based amphiphilic block

- copolymers: molecular design, self-assembly and biomedical applications”, *Mater. Sci. Eng.*: **C45**, 620-634.
- Lifson, S., Hagler, A.T. and Dauber, P. (1979), “Consistent force-field studies of inter-molecular forces in hydrogen-bonded crystals .1. Carboxylic-Acids, Amides, and the C=O...H- Hydrogen-Bonds”, *J. Am. Chem. Soc.*, **101**(18), 5111-5121.
- Lim, D.I., Park, H.S., Park, J.H., Knowles, J.C. and Gong, M.S. (2013), “Application of high-strength biodegradable polyurethanes containing different ratios of biobased isomannide and poly ( $\epsilon$ -Caprolactone) Diol”, *J. Bioact. Compatible Polym.*, **28**(3), 274-288.
- Maple, J.R., Dinur, U. and Hagler, A.T. (1988), “Derivation of force fields for molecular mechanics and dynamics from Ab initio energy surfaces”, *Proc. Natl. Acad. Sci. USA*, **85**(15), 5350-5354.
- Marcos-Fernández, A., Abraham, G.A., Valentín, J.L. and Román, J.S. (2006), “Synthesis and characterization of biodegradable non-toxic poly(Ester-Urethane-Urea)S based on Poly(E-Caprolactone) and Amino Acid Derivatives”, *Polymer.*, **47**(3): 785-798.
- Martina, M. and Hutmacher, D.W. (2007), “Biodegradable polymers applied in tissue engineering research: A review”, *Polym. Int.*, **56**(2), 145-157.
- Molecular Simulations, I. (1998), *Forcefield-based simulations, molecular simulations*, I. MSI Scientific Support and Customer Service 9685 Scranton Road San Diego, CA 92121-3752, MSI Documentation Group. Molecular Simulations, Inc. .
- Montanari, B., Ballone, P. and Jones, R.O. (1999), “Density functional study of Polycarbonate. 2. Crystalline Analogs, Cyclic Oligomers, and Their Fragments”, *Macromolecules*, **32**(10), 3396-3404.
- Niu, Y., Chen, K.C., He, T., Yu, W., Huang, S. and Xu, K. (2014), “Scaffolds from block polyurethanes based on Poly( $\epsilon$ -Caprolactone) (Pcl) and Poly(Ethylene Glycol) (Peg) for peripheral nerve regeneration”, *Biomater.*, **35**(14), 4266-4277.
- Ou, C.W., Su, C.H., Jeng, U.S. and Hsu, S.h. (2014), “Characterization of biodegradable polyurethane nanoparticles and thermally induced self-assembly in water dispersion”, *ACS Appl. Mater. Interfaces*, **6**(8), 5685-5694.
- Pandey, R.B., Heinz, H., Feng, J., Farmer, B.L., Slocik, J.M., Drummy, L.F. and Naik, R.R. (2009), “Adsorption of peptides (A3, Flg, Pd2, Pd4) on gold and palladium surfaces by a coarse-grained Monte Carlo simulation”, *Phys. Chem. Chem. Phys.*, **11**(12), 1989-2001.
- Plimpton, S. and Hendrickson, B. (1995), “Parallel molecular-dynamics algorithms for simulation of molecular-systems”, *Acs Sym. Ser.*, **592**, 114-132.
- Regis, S., Youssefian, S., Jassal, M., Phaneuf, M.D., Rahbar, N. and Bhowmick, S. (2014), “Fibronectin adsorption on functionalized electrospun Polycaprolactone scaffolds: Experimental and molecular dynamics studies”, *J. Biomedical Mater. Res. Part A*, **102**(6), 1697-1706.
- Sinha, V.R., Bansal, K., Kaushik, R., Kumria, R. and Trehan, A. (2004), “Poly- $\epsilon$ -Caprolactone Microspheres and Nanospheres: An overview”, *Int. J. Pharmaceutics*, **278**(1), 1-23.
- Studio., A.S.I.M. (2002-2016), Biovia Materials Studio 8.0, BIOVIA Materials Studio.
- Tatai, L., Moore, T.G., Adhikari, R., Malherbe, F., Jayasekara, R., Griffiths, I. and Gunatillake, P.A. (2007), “Thermoplastic biodegradable Polyurethanes: The effect of chain extender structure on properties and in-Vitro degradation”, *Biomater.*, **28**(36), 5407-5417.
- Tiwari, A. and Raj, B. (2015), *Reactions and mechanisms in thermal analysis of advanced materials*, Wiley.
- Uemura, T., Yanai, N., Watanabe, S., Tanaka, H., Numaguchi, R., Miyahara, M.T., Ohta, Y., Nagaoka, M. and Kitagawa, S. (2010), “Unveiling thermal transitions of polymers in Subnanometre Pores”, *Nat. Commun.*, **1**, 83.
- Vanommeslaeghe, K., Ghosh, J., Polani, N.K., Sheetz, M., Pamidighantam, S.V., Connolly, J.W.D. and MacKerell, A.D. (2011), “Automation of the charmm general force field for drug-like molecules”, *Biophys. J.*, **100**(3), 611-611.
- Vanommeslaeghe, K., Hatcher, E., Acharya, C., Kundu, S., Zhong, S., Shim, J., Darian, E., Guvench, O., Lopes, P., Vorobyov, I. and MacKerell, A.D. (2010), “Charmm general force field: A force field for drug-like molecules compatible with the Charmm all-atom additive biological force fields”, *J. Comput. Chem.*, **31**(4), 671-690.

- Vanommeslaeghe, K., Raman, E.P. and MacKerell, A.D. (2012), "Automation of the Charmm general force field (Cgenff) li: Assignment of bonded parameters and partial atomic charges", *J. Chem. Inf. Model.*, **52**(12), 3155-3168.
- Younes, H.M., Bravo-Grimaldo, E. and Amsden, B.G. (2004), "Synthesis, characterization and in Vitro degradation of a biodegradable elastomer", *Biomater.*, **25**(22), 5261-5269.
- Yu, W.B., He, X.B., Vanommeslaeghe, K. and MacKerell, A.D. (2012), "Extension of the Charmm general force field to Sulfonyl-containing compounds and its utility in biomolecular simulations", *J. Comput. Chem.*, **33**(31), 2451-2468.

DC